Available online at www.sciencedirect.com
SCIENCE DIRECT®
Journal of Power Sources 138 (2004) 351–359
JOURNAL OF POWER SOURCES
www.elsevier.com/locate/jpowsour

Physical and electrochemical characterization of activated carbons prepared from firwoods for supercapacitors

Feng-Chin Wu[a,*], Ru-Ling Tseng[b], Chi-Chang Hu[c], Chen-Ching Wang[c]

[a] *Department of Chemical Engineering, National United University, No. 1, Lien Da, Kung-Ching Li, Miao-Li 360, Taiwan*
[b] *Department of Safety, Health and Environmental Engineering, National United University, Miao-Li 360, Taiwan*
[c] *Department of Chemical Engineering, National Chung Cheng University, Chia-Yi 621, Taiwan*

Received 15 April 2004; accepted 14 June 2004
Available online 14 August 2004

Abstract

Activated carbons prepared from firwoods by means of a steam activation method at 900 °C for 1–7 h are demonstrated as promising materials for supercapacitors. The carbons exhibit high-power, low equivalent series resistance and highly reversible characteristics between −0.1 and 0.9 V in aqueous electrolytes. The pore structure of the carbons is systematically characterized by the *t*-plot method based on N_2 adsorption isotherms. The adsorption equilibria of tannic acid, methylene blue, 4-chlorophenol and phenol from aqueous solutions on such carbons are perfectly fitted by the Langmuir equation. All the steam-activated carbons prepared at different activation times (t_A) display ideal capacitive performance in aqueous media. This is attributed mainly to the development of mesopores (with an average pore diameter, D_p, between 2.68 and 3.04 nm), which depends strongly on t_A. The average specific capacitance of a steam-activated carbon with a t_A of 7 h, as estimated from cyclic voltammetic curves measured at 200 mV s^{-1}, reaches 120 F g^{-1} between −0.1 and 0.9 V in acidic electrolytes. The capacitive characteristics of steam-activated carbons in $NaNO_3$, H_2SO_4 and HNO_3 can be roughly determined by the adsorption data of species with suitable molecular weights. The results indicate that the observed increase in double-layer capacitance arises mainly from the development of mesopores.

Keywords: Activated carbon; Steam activation; BET surface area; Mesopores; Surpercapacitor

1. Introduction

Activated carbons are important materials that have been used in various industrial applications [1–5]. Recently, investigations on the porous structures and electrochemical behaviour of activated carbons in various forms have been carried out because of their use as electrode materials for surpercapacitors [1,6–8]. Since the cost of supercapacitors based on activated carbons is low [7], these devices are commercially attractive for many applications, such as mobile telecommunictions and starting and back-up power for hybrid electric vehicles [9]. On the other hand, for high-power purposes, the proportion of mesopores (i.e. pore diameter between 2 and 50 nm) within activated carbons is considered to be one of the key determinants of the capacitive performance of supercapacitors. This is because a complete array of the electric-double layers can be established and solvated ions can move freely within such pores. A high ratio of mesopores will, however, result in a loss of specific surface-area [8,10].

A large portion of electric energy stored in supercapacitors will be consumed during discharge if the equivalent series resistance (ESR) is significant, which usually results in a poor conductivity of the activated carbons as well as poor diffusion of solvated ions within the micropores [6,9,11]. These characteristics depend mainly on the nature, the BET surface-area, and the porous structure of carbons [6,9,10–12]. Accordingly,

* Corresponding author. Tel.: +886 37 381575; fax: +886 37 332397.
E-mail address: wfc@nuu.edu.tw (F.-C. Wu).

0378-7753/$ – see front matter © 2004 Elsevier B.V. All rights reserved.
doi:10.1016/j.jpowsour.2004.06.023

pore-size distribution is one of the key factors that dictate the selection of activate carbon materials for supercapacitors [6,7,9]. In fact, activated carbons manufactured under different conditions are found to have different pore structures and surface conditions, which generally restrict the electrochemical accessiblity of the BET surface-area [6,9–11]. In addition, for accessible surface areas, the specific capacitance ($\mu F\ cm^{-2}$) is not the same due to the presence of various functional groups [10,13]. Hence, several studies have been performed to modify the surface properties of activated carbons in order to optimize their capacitive performance, i.e. high-power, low ESR, and high specific capacitance [l,6–8,ll–13].

In general, activated carbon materials with unique pore-size distributions are attributable to the nature of the precursors and the various pre-treatments [10,14]. Highly electrochemically accessible surface-areas with mesoporous structures are the typical characteristics of activated carbons derived from wood products [2]. In our previous work [2,15,16], a series of studies were conducted to manufacture activated carbons with a unique pore-size distribution (from wood wastes) for application in industrial pollution control. Although agricultural or wood wastes have been used for preparing activated carbons via $ZnCl_2$ and H_3PO_4 treatment [3], an environmentally friendly steam-activation method is preferred on account of the resultant secondary pollution and chemical consumption. Accordingly, there have been many reports [2,15–25] of the preparation as well as the characterization of the physicochemical properties of wood-based activated carbon [2,15-25]. By contrast the relationship between the double-layer responses of solvated ions and the adsorption behaviour of chemicals within activated carbon has been rarely discussed [10].

The aim of this investigation is to prepare various activated carbons from firwoods and to evaluate their applicability in supercapacitors. In addition, the physical properties such as iodine number, BET surface-area, pore-size distribution, total pore volume and yield of steam-activated carbons are systematically characterized. Finally, a correlation between the adsorption behaviour of certain species and the capacitive performance of the electric double-layer on charge/discharge is attempted.

2. Experimental details

2.1. Preparation of activated carbons

After drying at 110 °C for 24 h, firwoods were placed in a sealed ceramic oven and heated at a rate of 5 °C min^{-1} to 550 °C. Steam generated from deionized water (Millipore, Milli-Q) in a heated tube was introduced into the oven at a rate of 3 cm^3 min^{-1} for 3 h. The firwoods were then thermally treated under an oxygen-deficient environment, which is a, so-called a carbonization process. In the subsequent activation process, the oven was further heated at the same rate to reach 900 °C under the same flow-rate of steam. The time for activation at 900 °C was varied from 1 to 7 h. The resultant carbons were ground in a mill, washed with pure water, dried, and finally sieved in the size range of 0.12–0.2 mm.

2.2. Measurements of physical properties

The pysical properties of activated carbons, including the iodine number, BET surface-area, and bulk density, were measured. The yield was calculated as the weight ratio of final carbons to the initial dried raw materials. The iodine number of the carbons (q_{iodine}) was measured at 30 °C based on the standard ASTM Designation D4607-86 test method. The BET surface-area of the carbons (S_p) was obtained from nitrogen adsorption isothersms at 77 K (Porous Materials, BET-202A). The total pore volume (V_{pore}) and the pore-size distribution were estimated by BJH theory [26], and the micropore volume (V_{micro}) and external surface area (S_{ext}) by means of the t-plot method [27–29]. The surface area of micropores (S_{micro}) was obtained by difference [30]. The bulk density was determined from the standard ASTM-D2854-89 test method.

2.3. Procedures for adsorption

Tannic acid (TA, M_w (molecular weight) = 1701), methylene blue (MB, M_w = 320), 4-chloropenol (4-CP, M_w = 128.5) and phenol (M_w = 94) were analytical reagent grade. The aqueous phase for adsorption was prepared with dissolving TA, MB, 4-CP and phenol in de-ionized water without pH adjustment. For the ranges of studies, the initial pH was about 3.52 for 500 g m^{-3} TA, 6.6 for 200 g m^{-3} MB, and 6.4 for 1 mol dm^{-3} phenol and 4-CP.

In the adsorption (equilibrium) experiments, 0.1 g carbon was added to a 0.1 dm^3aqueous phase solution in a 0.25 dm^3 flask and stirred for 5 days in a water bath at 30 °C. Preliminary tests showed that adsorption was complete after 4 days. After filtration with glass fibres total liquid-phase concentrations were analyzed with an UV–vis spectrophotometer (Hitachi U2000). The amount of adsorption at equilibrium, q_e (g kg^{-1}), was obtained by:

$$q_e = \frac{(C_0 - C_e)V}{W} \quad (1)$$

where: C_0 and C_e are the initial and equilibrium liquid-phase concentrations (g m^{-3}); V is the volume of the solution (m^3); W is the weight of dried carbons used (kg).

2.4. Electrode preparation

Activated carbon powders were well mixed with 2 wt.% polyvinylidene difluoride (PVdF) binders for 30 min and *N*-methyl-2-pyrrolidone (NMP) was dropped into the above mixture and ground to form the coating slurry. This slurry was smeared on to the pretreated graphite substrates and then dried in a vacuum oven at 50 °C overnight. In order to avoid any unexpected influences, the total amount of activated car-

bon paste on each electrode was kept approximately constant (ca. 2 mg cm^{-2}). The 10 mm × 10 mm × 3 mm graphite substrates before coating with activated carbons were first abraded with ultrafine SiC paper, degreased with acetone and water, then etched in a 0.1 M HCl solution at room temperature (ca. 26 °C) for 10 min, and finally degreased with water in an ultrasonic bath. The exposed geometric area of these pretreated graphite supports is equal to 1 cm^2, while the other surface areas were insulated with PTFE (polytetrafluorene ethylene) coatings.

2.5. Capacitance measurements

Electrochemical measurements were performed by means of an electrochemical analyzer system, CHI 633A (CH Instruments). All experiments were carried out in a three-compartment cell. An Ag/AgCl electrode (Argenthal, 3 M KC1, 0.207 V versus SHE at 25 °C) was used as the reference electrode and a platinum wire with an exposed area equal to 4 cm^2 was employed as the counter electrode. A Luggin capillary was used to minimize errors due to *i*R drop in the electrolytes. The electrolytes used for the capacitive characterization were degassed with purified nitrogen gas before measurements for 25 min and this nitrogen was passed over the solutions during the measurements. The solution temperature was maintained at 25 °C by means of a water thermostat (Haake DC3 and K20).

3. Results and discussion

3.1. Physical properties of steam-activated carbons

According to the definition from IUPAC, pores contained in activated carbons are classified into three groups: micropores (pore size < 2 nm), mesopores (2–50 nm) and macropores (>50 nm). In addition, micropores usually account for over 95% of the total surface area for common activated carbons [31].

Adsorption/desorption isotherms of N_2 at 77 K on steam-activated carbons prepared at different activation times (t_A) are shown in Fig. 1. Note that for all isotherms, adsorption and desorption lines overlap completely in the low relative-pressure region while the hysteresis loop exists in the high relative-pressure region (P/P_0 > 0.5), which is mainly due, among other factors such as the slit-shaped pores, to the presence of ink-bottle types of pores [32]. According to the Kelvin equation [33], the ink-bottle type of pores have a larger pore size in the bottle body, which results in the occurrence of hysteresis in the high relative-pressure region. From a comparison of these isotherms, a larger amount of adsorption and a wider hysteresis loop is found for the carbons prepared at a longer t_A. This indicates the existence of a larger amount of porous spaces and ink-bottle pores.

The pore-size distributions of steam-activated carbons with t_A equal to 1, 3, 5, and 7 h are presented as curves 1–4 in Fig. 2. These curves generally show that the pores distributed within these steam-activated carbons are mainly composed of two groups: micro-pores with pore diameters < 2.0 nm and mesopores with pore diameters centered at 4.0 nm. In addition, the amount of micropores gradually increases with t_A, while mesopores with pore diameters from 2 to 4 nm steadily develop. Moreover, mesopores with pore diameters ≥ 4.6 nm are gradually formed with increasing t_A. Accordingly, the development of micropores and mesopores within wood-based carbons can be easily achieved by the steam-activation method.

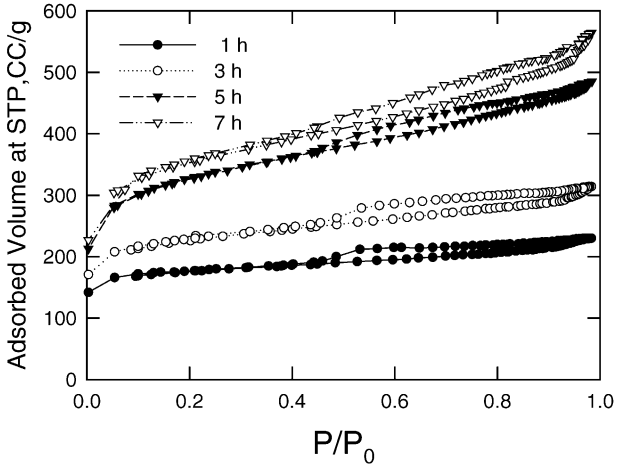

Fig. 1. Adsorption–desorption isotherms of N_2 at 77 K on steam-activated carbons prepared at different t_A.

The pore properties of steam-activated carbons, including S_p, S_{ext}, S_{micro}/S_p, V_{pore}, V_{micro}, V_{micro}/V_{pore} and q_{iodine}, are listed in Table 1. The iodine number, q_{iodine}, is a measure

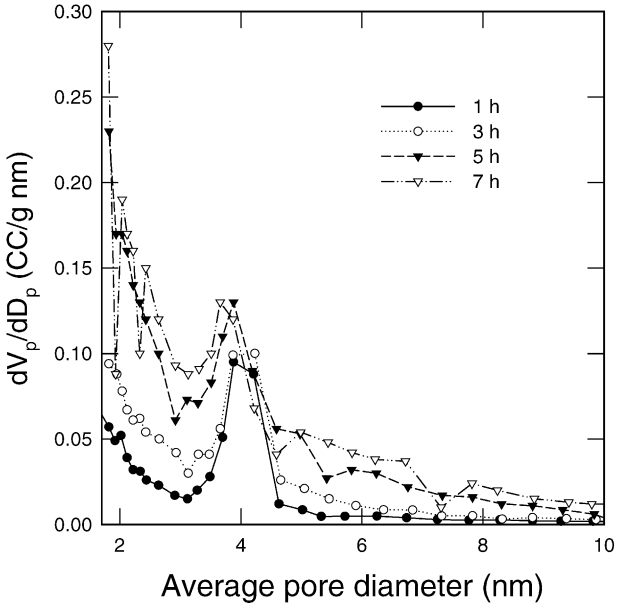

Fig. 2. Pore-size distributions of steam-activated carbons with t_A of (1, —●—) 1 (2, —○—) 3 (3, —▼—) 5 and (4, —▽—) 7 h.

Table 1
Physical properties of steam-activated carbons prepared from firwoods at different activation times

t_A(h)	S_p ($m^2\,g^{-1}$)	S_{ext} ($m^2\,g^{-1}$)	S_{micro}/S_p	V_{pore} ($cm^3\,g^{-1}$)	V_{micro} ($cm^3\,g^{-1}$)	V_{micro}/V_{pore}	q_{iodine} ($g\,kg^{-1}$)
1	528	78.6	0.861	0.354	0.236	0.667	762
3	699	126.7	0.819	0.483	0.295	0.611	851
5	1016	317.8	0.731	0.747	0.377	0.505	962
7	1131	322.2	0.715	0.868	0.392	0.476	1018

of adsorption ability for low-M_w species [34]. As shown in Table 1, q_{iodine} increases from 762 to 1067 g kg^{-1} when t_A is changed from 1 to 7 h. These values are comparable with those of commercially-available activated carbons, e.g. 650 (ICI Hydrodarco 3000), 900 (Calgon Filtrasorb 300), 950 (Westvaco Nuchar WL), and 1000 g kg^{-1} (Witco 517). In addition, the iodine numbers of activated carbons prepared from apricot stones, grape seeds and cherry stones are 894, 607 and 907 g kg^{-1}, respectively [28]. From Table 1, prolonging t_A leads to an increase in S_p, S_{ext}, V_{pore}, and V_{micro} but causes a decrease in S_{micro}/S_p and V_{micro} V_{pore} The former results indicate that the number of pores increases with prolonging t_A, meanwhile the latter reveal that an increase in S_p gives a significant creation of mesopores. Based on these findings and the discussion on Fig. 2 and Table 1, steam activation is mainly used to develop mesopores within wood-based carbons. Note that, the highest S_p for the carbon prepared in this work (1131 $m^2\,g^{-1}$) is comparable with those for commercial ones; for example, 300–600 (ICI Hydrodarco 3000), 1044 (Calgon Filtrasorb 400), 1000 (Westvaco Nuchar WL), and 1050 $m^2\,g^{-1}$ (Witco 517). On the other hand, some activated carbons prepared by chemical activation reach above 2500 $m^2\,g^{-1}$ [35,36]. In addition, carbons prepared from apricot stones, grape seeds and cherry stones have an S_p of 1175,487 and 836 $m^2\,g^{-1}$, respectively [34].

The dependence of D_p (average diameter of pores, $4V_{pore}/S_p$), bulk density and yield of activated carbons on S_p is shown in Fig. 3. It is evident that under the range of investigation, the yield and bulk density of carbons decrease with increasing S_p. These data further support statement that porosity development can be easily achieved by prolonging the t_A of steam activation. By contrast, D_p increases from 2.68 to 3.04 (nm) when S_p is increased from 528 to 1130 $m^2\,g^{-1}$. This further supports the finding that steam activation is used mainly to develop mesopores within wood-based carbons. Also note that these D_p data are comparable with those of commercially available activated carbons (0.912–2.30 nm), such as 0.912 (Spectracorp M-10), 1.473 (Spectracorp M-20), 2.23 (Calgon F400), 2.0 (Barney Cheney SK1301), 1.90 (Westvaco Nuchar MV-L) and 2.30 nm (Westvco WV-DC). In addition, the average pore diameter of activated carbons prepared from coconut shells, palm seeds, bagasse and plum kernel are 2.1, 2.43, 1.46 and 2.39 nm, respectively [2,16,37]. Due to the fact that the D_p values of activated carbons prepared in this work are relatively large (from 2.68 to 3.04 nm), these carbons are expected to be of practical potential in the application of supercapacitors [36].

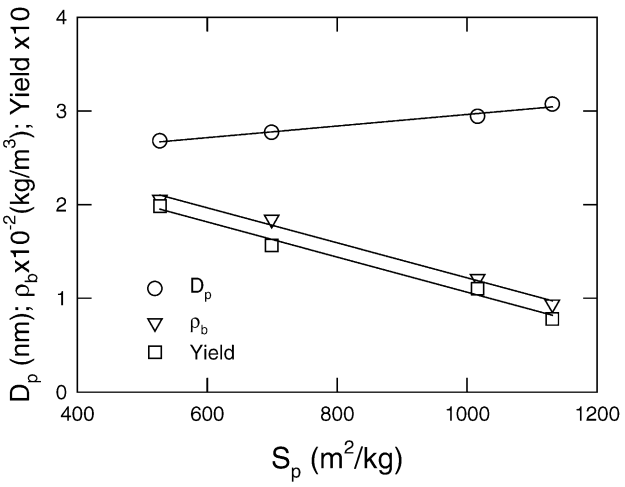

Fig. 3. Mean pore size (D_p), bulk density, and yield of steam-activated carbons with different BET surface–areas.

3.2. Equilibrium adsorption on steam-activated carbons

The adsorption isotherm is important to describe how solutes interact with adsorbents, which is critical in optimizing the use of adsorbents. In addition, the movement/adsorption of solvated charged species and oriented dipoles that exist at the activated carbon–electrolyte interface may be predicted by the adsorption behaviour of solutes of different sizes within activated carbons. Accordingly, adsorption isotherms of chemicals in different molecular weights are investigated in this work.

Typical equilibrium adsorption of TA, MB, 4-CP and phenol at 30 °C on activated carbons prepared with t_A = 7 h is shown in Fig. 4. It is obvious that the adsorption capacity of activated carbon (based on g kg^{-1}) decreases with decreasing molecular weight of the solutes (i.e. TA > MB > 4-CP > phenol). On the other hand, an opposite trend is obtained if the adsorption ability is estimated on the basis of molecules/moles being adsorbed (i.e. mole kg^{-1}). Note that, correlation of isotherm data by theoretical or empirical equations is essential to practical operation. The widely used Langmuir equation is given as:

$$\frac{C_e}{q_e} = \frac{1}{K_L q_{mon}} + \frac{1}{q_{mon}} C_e \quad (2)$$

where q_{mon} is the amount of adsorption (in g kg^{-1}) that corresponds to complete monolayer coverage and K_L is the Langmuir constant. Linear plots of (C_e/q_e) against C_e give K_L and

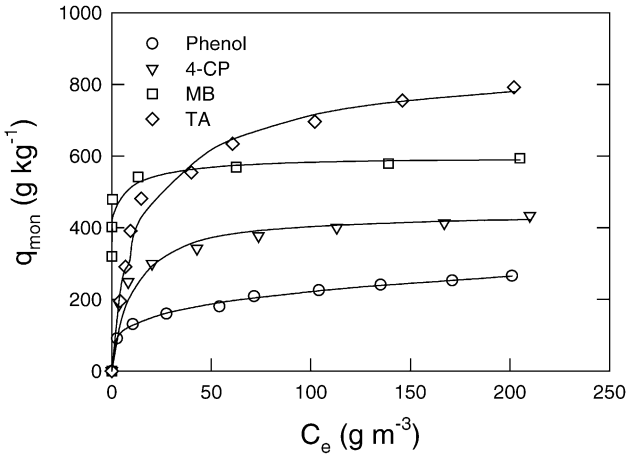

Fig. 4. Adsorption isotherms of solutes at 30 °C on steam-activated carbons with t_A of 7 h.

q_{mon}, as shown in Fig. 5(a) and (b). The parameters (listed in Table 2) estimated from Fig. 5 are reliable since the fitting for TA, MB, 4-CP and phenol adsorption on all activated carbons in the concentration range of study is excellent (correlation coefficient, $R^2 > 0.988$). The adsorption capacity (q_{mon}) of TA and MB increases with increasing S_p. At S_p = 1131 m^2 g^{-1}, the values of q_{mon} for TA and MB are 831 and 590 g kg^{-1}, respectively, which are larger than those obtained earlier in similar solute–adsorbent systems [2,4,15,38]. By contrast, the values of q_{mon} for phenol and 4-CP increase only slightly with increasing S_p.

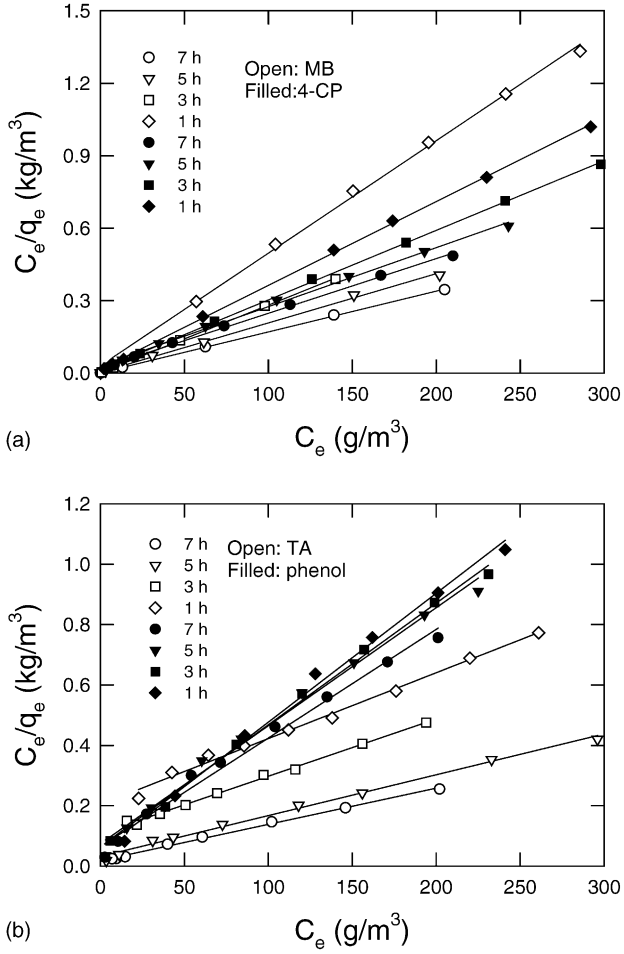

Fig. 5. Plots of (C_e/q_e) against C_e (tests of Langmuir equation) for adsorption of (a) MB and 4-CP and (b) TA and phenol on steam-activated carbons with different t_A.

Table 2
Parameters in isotherm equations obtained at 30 °C on steam-activated carbons with different BET surface areas

Adsorbate	S_p (m^2 g^{-1})	K_L (m^3 g^{-1})	q_{mon} (g kg^{-1})	R^2
TA	527	0.011	412	0.995
	699	0.018	527	0.996
	1016	0.043	740	0.994
	1131	0.069	831	0.997
MB	527	0.154	215	0.998
	699	1.561	360	1.000
	1016	0.636	490	0.998
	1131	2.496	590	1.000
4-CP	527	0.163	295	0.998
	699	0.207	346	1.000
	1016	0.077	413	0.996
	1131	0.109	441	0.998
Phenol	527	0.086	234	0.995
	699	0.105	239	0.994
	1016	0.053	255	0.997
	1131	0.056	278	0.998

3.3. Capacitive characteristics of steam-activated carbons

Based on the fact that the D_p of steam-activated carbons is located between 2.68 and 3.04 nm, these carbons should be suitable for supercapacitors. Accordingly, the electrochemical behaviour of steam-activated carbons with different t_A has been measured to demonstrate this unique characteristic. Typical results for steam-activated carbons with t_A of 1, 3, 5, and 7 h measured in 1 M HNO_3 at 25 mV s^{-1} are shown in Fig. 6 as curves 1–4, respectively. There is a pair of wide peaks on all curves between 0 and 0.5 V. These are attributed to the presence of a redox couple in this potential region [10]. In addition, all *i–E* curves on the positive sweeps are symmetical with those on the corresponding negative sweeps, which indicates that all carbons show the excellent capacitive property in HNO_3. In addition, voltammetric currents gradually increase with extending the activation time which can be attributed to the fact that the specific surface of activated carbons is increased with t_A (see Table 1). The voltammetric currents rapidly reach their respective plateau values for all curves when the direction of the potential sweep is changed, although the scan rate is as fast as 25 mV s^{-1}. These results indicate a low ESR for all carbons with different t_A. A low ESR should come from a combination of a high electronic conductivity of electrode materials (i.e. steam-activated carbons) and a low ionic resistance of the electrolyte within the pores of activated carbons during the charge–discharge tests.

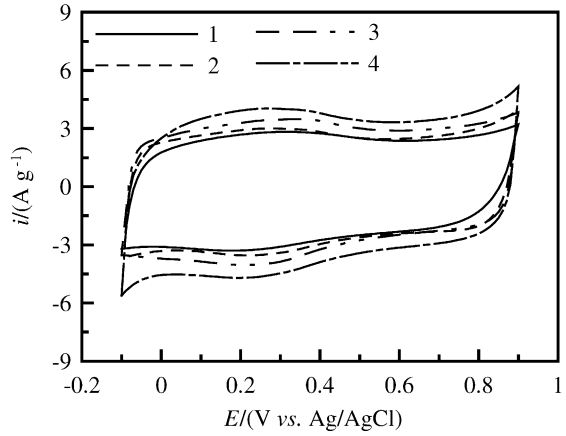

Fig. 6. Cyclic voltammograms of steam-activated carbons with t_A of (1) if (2) 3 (3) 5 and (4) 7 h. All curves were measured at 25 mV s^{-1} in 1.0 M HNO_3.

The latter result is probably due to the presence of a large portion of mesopores within all the activated carbons prepared in this work. From all the above results and discussion, steam-activated carbons from firwoods with t_A from 1 to 7 h offer potential application in supercapacitors.

Typical cyclic voltammograms of activated carbon with a t_A of 5 h measured in 1 M $NaNO_3$, 1 M HNO_3, and 0.5 M H_2SO_4 are shown in curves 1–3 of Fig. 7, respectively in curve 1, high background currents without obvious redox currents are clearly found on both positive and negative sweeps over the whole potential range of investigation. This capacitive-like and symmetric *i*–E response indicates that steam-activated carbons exhibit excellent electrochemical characteristics for supercapacitors in 1 M $NaNO_3$. Since the voltammetric charges on the positive and negative sweeps are approximately equal, the good reversibility of the double-layer charge–discharge characteristics for this steam-activated carbon further supports its consideration for supercapacitors. On curve 2, larger background currents

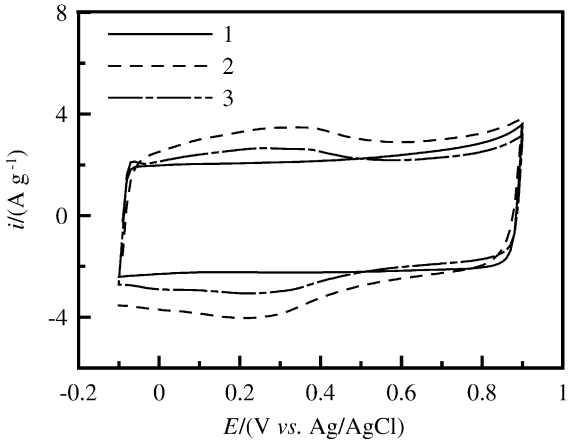

Fig. 7. Cyclic voltammograms of steam-activated carbon with t_A of 5 h in (1) 1 M $NaNO_3$ (2) 1 M HNO_3 and (3) 0.5 M H_2SO_4. All curves were measured at 25 mV s^{-1}.

with a pair of broad redox peaks negative to 0.6 V are clearly found. This symmetrical *i*–E response is also found for other carbons with different t_A (see Fig. 6), which demonstrates that the steam-activated carbons prepared in this work show ideal capacitive performance in both acidic and neutral media, which is different from the activated carbon fabrics studied in our previous work [39]. Similar voltammetric responses of this steam-activated carbon are obtained in H_2SO_4 although lower voltammetric currents on both positive and negative sweeps are clearly observed on curve 3, especially in the more positive potential region.

The above differences in voltammetric currents obtained in different electrolytes are attributed to a combination of two reasons. First, the lower capacitive current of curve 3 in comparison with that on curve 2 is due to the larger ionic solvation radius of SO_4^{2-} because of its higher charge density and the larger atom number in comparison with NO_3^-. Second, on the basis of the proton-hopping mechanism in aqueous media [40], the capacitive currents measured in acidic solutions are reasonably larger than those in nearly neutral media (i.e. the voltammetric charge associated with curve 1 is the smallest). All these observations demonstrate that the double-layer capacitance of steam-activated carbons is a strong function of the electrolyte employed. In addition, the capacitive characteristics of these carbons in $NaNO_3$ are better than those in acidic media since the voltammetric currents obtained in the former electrolyte are approximately independent of the electrode potential. Based on specific capacitance, however, carbons in acidic electrolytes give larger capacity in energy storage since all steam-activated carbons show good reversibility of charge–discharge in both acidic and neutral media.

Data for the specific capacitance of various steam-activated carbons measured in 1 M $NaNO_3$, 1 M HNO_3 and 0.5 M H_2SO_4 are listed in Table 3. These were estimated from cyclic voltammograms measured at 25 mV s^{-1}. All capacitance data have been corrected for the capacitive contribution of graphite substrates although this contribution is negligible. From columns 2–4, it is seen that the specific capacitance is monotonously increased with prolonging the activation time. This is attributed to an increase in the BET surface-area as well as the proportion of mesopores. In addition, the sequence of electrolytes with respect to decreasing the specific capacitance of steam-activated carbons is: HNO_3 > H_2SO_4

Table 3
Specific capacitance of steam-activated carbons with different t_A in various electrolytes

t_A (h)	C_s (F g^{-1})		
	$NaNO_3$	HNO_3	H_2SO_4
1	41	96	75
3	82	97	89
5	89	120	96
7	114	142	142

All specific capacitances were obtained from CV curves measured at 25 mV s^{-1}

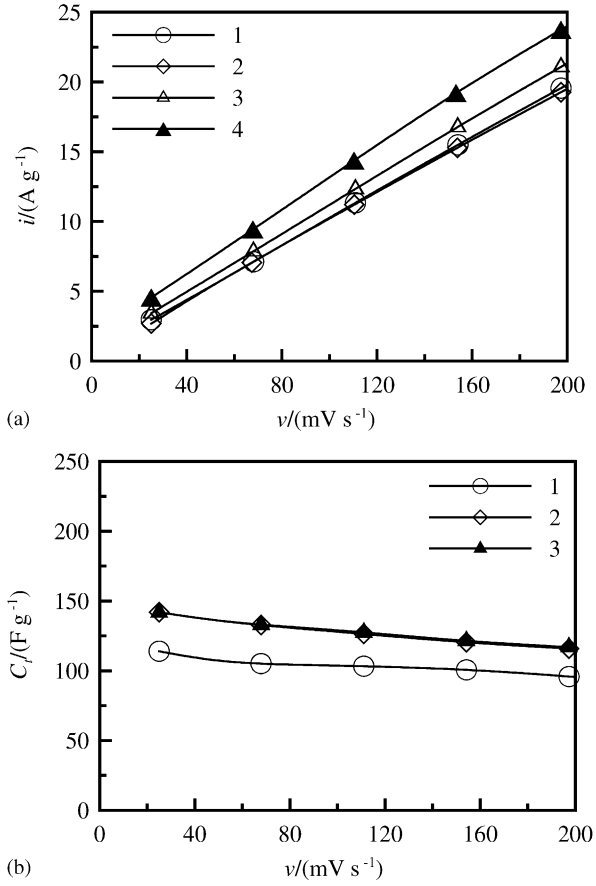

Fig. 8. (a) Dependence of voltammetric currents on scan rate of voltammograms where currents are obtained at (1) 0.2 (2) 0.4 (3) 0.6 and (4) 0.8 V on the positive sweep in 1 M $NaNO_3$. (b) Dependence of specific capacitance on scan rate in (1) 1 M $NaNO_3$ (2) 1 M HNO_3 and (3) 0.5 M H_2SO_4. All data obtained for steam-activated carbon with t_A of 7 h.

> $NaNO_3$ when the steam activation time is specified. Such a finding supports the proposal that the double-layer capacitance of steam-activated carbons is a strong function of the selected electrolyte.

The dependence of voltammetric currents obtained at 0.2, 0.4, 0.6 and 0.8 V during positive scans for the steam-activated carbon with t_A of 7 h on the scan rate of the voltammogram (V) in 1 M $NaNO_3$ is shown in Fig. 8(a)) as lines 1–4, respectively. In addition, the dependence of specific capacitance on the scan rate in 1 M $NaNO_3$, 1 M HNO_3 and 0.5 M H_2SO_4 is shown in Fig. 8(b) as curves 1–3, respectively. In Fig. 8(a), all lines are linear, which indicates the fact that the double-layer charge–discharge currents are linearly dependent on the scan rates. This typical capacitive behaviour indicates the highly reversible charge–discharge responses of the electric double-layers, which meets one of the basic requirements of electrode materials for supercapacitors (i.e. high-power property). In Fig. 8(b), an obvious decrease in specific capacitance of this steam-activated carbon with increasing the scan rate is clearly found on curves 2 and 3, but is less obvious for curve 1. These results suggest that the specific capacitance of steam-activated carbons

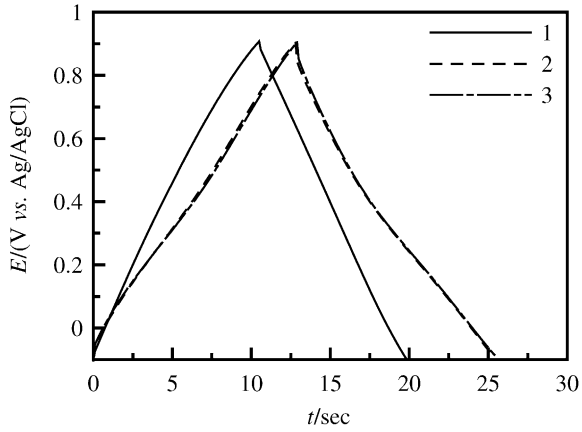

Fig. 9. Chronopotentiograms of steam-activated carbon with t_A of 7 h measured at 10 A g^{-1} in (1) 1 M $NaNO_3$ (2) 1 M HNO_3 and (3) 0.5 M H_2SO_4.

in acidic media is significantly decreased with increasing the scan rate. Thus, it can be conducted that certain micropores that are partially accessible by acidic electrolytes should not provide double-layer capacitance when $NaNO_3$ is employed. These micropores, which are partially accessible due to proton hopping, cannot provide double-layer capacitance under a high charge–discharge rate since the establishment of electric double-layers may be not as complete/fast as the rate of potential change (i.e. scan rate). This is especially true for the inner surface areas of micropores which are not freely accessible for solvated ions.

Chronopotentiograms for steam-activated carbon with t_A of 7 h measured at 10 A g^{-1}in 1 M $NaNO_3$, 1 M HNO_3 and 0.5 M H_2SO_4 are presented in curves 1–3 of Fig. 9, respectively. The average specific capacitance of this carbon material measured at this high current density can be calculated on the basis of Eq. (1) [39,41–45]:

$$C_s = \frac{C}{w} = \frac{i}{|(dE/dt)|} \approx \frac{i}{(\Delta E/\Delta t) \times w} \quad (3)$$

where C_s, C, w, and (dE/dt) indicates the specific capacitance, average capacitance, weight of carbon, current density of charge–discharge and slope of the charge–discharge curves at a specific time. In this work, the slopes of the curves at a specific time are very close to their mean values $(\Delta E/\Delta t)$ since all charge curves are linear and symmetrical, to their corresponding discharge curves. The specific capacitance of this carbon obtained in 1 M $NaNO_3$,1 M HNO_3 and 0.5 M H_2SO_4 is equal to about 91, 118 and 118 F g^{-1}, respectively. These values are lower than those measured at 25 mV s^{-1} by cyclic voltammetry (see Table 3). This is indicative of a significant decrease in specific capacitance under a very high current density of charge–discharge (similar to the situation in Fig. 8(b)), which is a probably due to a significant content of micropores within the steam-activated carbon (see Fig. 2 and Table 1). Since the iR drop obtained on all discharge curves under this high current density is small, the ESR on this electrode should also be very small, which is attributable to the good conductivity and mesoporous nature

of this steam-activated carbon (see Table 1). Moreover, since all *E–t* curves are symmetrical, the steam-activated carbons exhibit the high-power characteristics required by supercapacitors in all the aqueous solutions studied in this work.

3.4. Relationship between adsorption of chemicals and capacitive characteristics of steam-activated carbons

Based on the fact that the charge–discharge of electric double-layers is attributed to the movement/adsorption of solvated charged species and oriented dipoles at the activated carbon–electrolyte interface, the capacitive performance of activated carbons should be reasonably correlated to the adsorption behaviour of solutes of different sizes in aqueous media, although the adsorption isotherms of species are based on thermodynamic rather than kinetic viewpoints. Note that the double-layer capacitance is mainly determined by the accessible surface area that should be generally proportional to the active sites provided for the adsorption of organics [46]. In addition, both specific capacitance and adsorption capacity of activated carbons are found to increase with t_A, which further supports this opinion. Accordingly, three-dimensionless parameters for the specific surface-area (denoted as σ), the adsorption capability of organics (denoted as θ) and the specific capacitance (denoted as ε) are defined here to correlate the adsorption behaviour of species with the capacitive responses of electric double layers, namely:

$$\sigma = \frac{S_{p,t}}{S_{p,7}} \tag{4}$$

$$\theta = \frac{q_{mon,t}}{q_{mon,7}} \tag{5}$$

$$\varepsilon = \frac{C_{s,t}}{C_{s,7}} \tag{6}$$

where the additional subscripts *t* and 7 indicate the steam activation time. Based on the above definitions, the dependence of θ for TA, MB, 4-CP and phenol, as well as the dependence of ε for $NaNO_3$, HNO_3 and H_2SO_4 on σ are shown in Fig. 10(a) and (b), respectively. These data reveal several important features. First, the slopes of the four lines in Fig. 10(a) that correspond to TA, MB, 4-CP, and phenol are equal to 0.936, 1.106, 0.607 and 0.271, respectively. These slopes are lower than 1.391 that corresponds to the slope for the dependence of dimensionless mesopore volume on σ. In addition, the slope for the dependence of the dimensionless micropore volume on σ is equal to 0.751. These results indicate that the development of mesopores favours the adsorption of molecules with large molecular weights (e.g. TA and MB), while the increase in S_p in both mesopores and micropores only slightly increases the adsorption capability of small molecules (e.g. 4-CP and phenol). Although the slope for TA should be larger than that for MB, an opposite result is found. This suggests that the dependence of adsorption capability for organics is not a simple function of the molecular size. Second, in Fig. 10(b), the slopes of

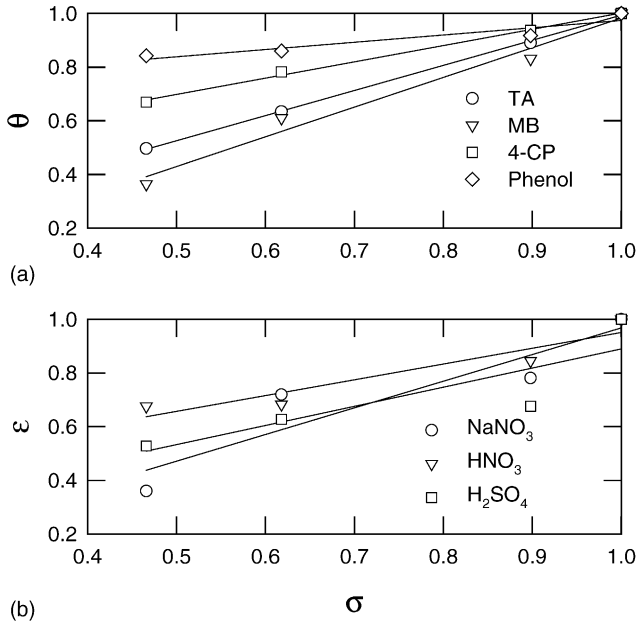

Fig. 10. Dependence of dimensionless (a) adsorption capability (θ) and (b) specific capacitance (ε) on the dimensionless specific surface-area (σ) of steam-activated carbons.

the three lines for $NaNO_3$, HNO_3 and H_2SO_4 are equal to 0.994, 0.589 and 0.713, respectively. The slope for $NaNO_3$ is close to that for TA and MB, which indicates that the behaviour of solvated ions arrangement/movement within meso-/micropores during the charge–discharge process is similar to the adsorption behaviour of large molecules. This is probably due to the fact that whole electric double-layers can be completely established within mesopores, which favours movement/rearrangement of solvated nitrate and sodium ions. Accordingly, the double-layer behaviour in $NaNO_3$ solution seems to be predicted by the adsorption of large molecules. Third, the sequence of electrolytes with respective to decreasing the slope is: $NaNO_3$ > H_2SO_4 > HNO_3. This sequence is predicable since the rate of proton hopping in aqueous solutions is much higher than that in other solvated ions [40], and the movement/arrangement rate of solvated SO_4^{2-} is slower than that of solvated NO_3^- [39]. The rate of proton hopping in aqueous media within meso-/micropores should be faster than the adsorption/movement of small molecules, whereas the adsorption of organics is at an equilibrium situation. Thus, the influence of protons on the capacitive behaviour is presumably similar to the adsorption behaviour of small molecules such as phenol. Accordingly, the slopes of ε against σ obtained from HNO_3 and H_2SO_4 solution should be much lower than that measured in $NaNO_3$ since the double-layer charge–discharge involves the arrangement and movement of solvated anions as well as the proton hopping in acidic electrolytes.

From all the above results and discussion, it can be concluded that the larger is radius of the solvated ion has, the larger is the slope of ε against σ. In addition, the dependence of specific capacitance measured in different elec-

trolytes on the specific surface-area and the pore-size distribution of steam-activated carbons can be reasonably estimated by the adsorption data of species with suitable molecular weights.

4. Conclusions

Activated carbons prepared from firwoods by means of the steam activation method for 1–7 h, exhibit excellent capacitive performance, i.e. high-power, low ESR, and high reversible characteristics between −0.1 and 0.9 V in aqueous electrolytes. Thus, they are promising electrode materials for supercapacitors. The mesoporous nature of these activated carbons with D_p from 2.68 to 3.04 nm, characterized by the *t*-plot method based on N_2 adsorption isotherms, is responsible for the ideal capacitive properties. These properties are strongly dependent on the activation time in steam. The average specific capacitance of a steam-activated carbon with t_A of 7 h (estimated cyclic voltammograms at 200 mV s^{-1}) can reach ∼120 F g^{-1} between −0.1 and 0.9 V in acidic electrolytes. The capacitive characteristics of steam-activated carbons in $NaNO_3$, H_2SO_4, and HNO_3 can be roughly estimated from the adsorption data of species with suitable molecular weights. The capacitive behaviour contributed by protons is similar to the adsorption behaviour of small molecules, such as phenol. The arrangement/movement of solvated ions within activated carbons is similar to the adsorption behaviour of large molecules such as TA and MB.

Acknowledgment

Financial support for this work, partially provided by the National Science Council of the Republic of China under contract no. NSC 92-221 l-E-239-006 and NSC 92-2214-E-194-005, is gratefully acknowledged.

References

[1] H. Shi, Electrochim. Acta 41 (1996) 1633.
[2] R.-L. Tseng, F.-C. Wu, R.-S. Juang, Carbon 41 (2003) 487.
[3] W.-T. Tsai, C.-Y. Chang, S.-L. Lee, Carbon 35 (1997) 1198.
[4] C.-T. Hsieh, H. Teng, Carbon 38 (2000) 863.
[5] H. Fujimoto, A. Mabuchi, K. Tokumitsu, T. Kasuh, Carbon (2000) 871.
[6] B.E. Conway, Electrochemical Supercapacitors, Kluwer–Plenum Publishing Co., NY, USA, 1999.
[7] L. Bonnefoi, P. Simon, J.F. Fauvarque, C. Sarrazin, J.F. Sarrau, A. Dugast, J. Power Sources 80 (1999) 149.
[8] D. Qu, H. Shi, J. Power Sources 74 (1998) 99.
[9] A. Burke, J. Power Sources 9l (2000) 37.
[10] K. Kinoshita, Carbon Electrochemical and Physicochemical Properties, Wiley, NY, USA, 1988.
[11] C. Niu, E.K. Sichel, R. Hoch, D. Moy, H. Tennent, Appl. Phys. Lett. 70 (1997) 1480.
[12] J. Gamby, P.L. Taberna, P. Simon, J.F. Fauvarque, M. Chesneau, J. Power Sources 101 (2001) 109.
[13] D. Qu, J. Power Sources 109 (2002) 403.
[14] R.L. McCreery, K.K. Cline, in: P.T. Kissinger, W.R. Heineman (Eds.), Laboratory Techniques in Electroanalytical Chemistry, Marcel Dekker, NY, USA, 1996 (Chapter 10).
[15] F.-C. Wu, R.-L. Tseng, R.-S. Juang, J. Hazard. Mater. B69 (1999) 287.
[16] R.-S. Juang, F.-C. Wu, R.-L. Tseng, J. Colloid Interface Sci. 227 (2000) 437.
[17] A. Cameron, J.D. MacDowall, Principles and Applications of Pore Structural Characterization, in: Proceedings of the RILEM/CNR International Symposium, 1985, pp. 251–275, , Milan, Italy.
[18] M.F. Tennant, D.W. Mazyck, Carbon 41 (2003) 2195.
[19] V. Minkova, S.P. Marinov, R. Zanzi, E. Bjornbom, T. Budinova, M. Stefanova, L. Lakov, Fuel Process. Technol. 62 (2000) 45.
[20] H. Benaddi, T.J. Bandosz, J. Jagiello, J.A. Schwarz, J.N. Rouzaud, D. Legras, F. Beguin, Carbon 38 (2000) 669.
[21] J. Pastor-Villegas, C. Valenzuela-Calahorro, V. Gomez-Serrano, Biomass Bioenerg. 6 (1994) 453.
[22] A. Mitomo, T. Sato, N. Kobayashi, S. Hatano, Y. Itaya, S. Mori, J. Chem. Eng. Jpn 36 (20031050).
[23] I. Abe, T. Fukuhara, S. Iwasaki, K. Yasuda, K. Nagagawa, Y. Iwata, H. Kominami, Y. Kera, Carbon 39 (2001) 1485.
[24] V. Minkova, M. Razvigorova, E. Bjornbom, R. Zanzi, T. Budinova, N. Petrov, Fuel Process. Technol. 70 (2001) 53.
[25] K. Babel, Adsorpt. Sci. Technol. 21 (2003) 363.
[26] E.P. Barrett, L.G. Joyner, P.P. Halenda, J. Am. Chem. Soc. 73 (1951) 373.
[27] J.H. de Boer, B.C. Lippens, B.G. Linsen, J.C.P. Broekhoff, A. van den Heuvel, T.J. Osiga, J. Colloid Interface Sci. 21 (1966) 405.
[28] K.S.W. Sing, D.H. Everett, R.A.W. Haul, L. Moscou, R.A. Pierotti, J. Rouquerol, Pure Appl. Chem. 57 (1985) 603.
[29] K.S.W. Sing, Carbon 27 (1989) 5.
[30] E.F. Sousa-Aguilar, A. Liebsch, B.C. Chaves, A.F. Costa, Micropor. Mesopor. Mater 25 (1998) 185.
[31] M.S. El-Geundi, Adsorpt. Sci. Technol. 15 (1997) 777.
[32] D.M. Ruthven, Principles of Adsorption and Desorption Processes, Wiley, NY, USA, 1984 (p. 55–58).
[33] R.B. Anderson, Experimental Methods in Catalytic Research, vol. 1, Academic Press, NY, USA, 1968.
[34] K. Gergova, N. Petrov, V. Minkova, J. Chem. Technol. Biotechnol. 56 (1993) 78.
[35] T.-C. Weng, H. Teng, J. Electrochem. Soc. 148 (2001) A368.
[36] H. Tamai, M. Kouzu, M. Morita, H. Yasuda, Electrochem. Solid State Lett. 6 (2003) A214.
[37] Z. Hu, M.P. Srinivasan, Micropor. Mesopor. Mater. 3 (2001) 267.
[38] G.M. Walker, L.R. Weatherley, Chem. Eng. J. 8 (2001) 201.
[39] C.-C. Hu, C.-C. Wang, J. Power Sources 125 (2004) 299.
[40] A. Bard, L.R. Faulkner, Electrochemical Methods, Fundamentals and Applications, Wiley, NY, USA, 1980.
[41] C.-C. Hu, Y.-H. Huang, J. Electrochem. Soc. 146 (1999) 2465.
[42] C.-C. Hu, K.-H. Chang, Electrochim. Acta 45 (2000) 2685.
[43] C.-C. Hu, Y.-H. Huang, Electrochim. Acta 46 (2001) 3431.
[44] C.-C. Hu, T.-W. Tsou, Electrochem. Commun. 4 (2002) 105.
[45] C.-C. Hu, C.-C. Wang, J. Electrochem. Soc. 150 (2003) 1079.
[46] C.-T. Hsieh, H. Teng, Carbon 38 (2000) 863.